A Detailed Study of Electronic and Dynamic Properties of Noble Gas–Oxygen Molecule Adducts

Caio Vinícius Sousa Costa [1], **Guilherme Carlos Carvalho de Jesus** [1], **Luiz Guilherme Machado de Macedo** [2], **Fernando Pirani** [3,4] and **Ricardo Gargano** [1,*]

1. Instituto de Física, Universidade de Brasília, Brasília 70297-400, DF, Brazil
2. Universidade Federal de São João del Rei, Divinópolis 35501-296, MG, Brazil
3. Dipartimento di Chimica, Biologia e Biotecnologie, Universitá degli studi di Perugia, Via Elce di Sotto 8, 06123 Perugia, Italy
4. Istituto CNR di Scienze e Tecnologie Chimiche (CNR-SCITEC), Via Elce di Sotto 8, 06123 Perugia, Italy
*   Correspondence: gargano@unb.br

Abstract: In this work, the binding features of adducts formed by a noble gas (Ng = He, Ne, Ar, Kr, Xe, and Rn) atom and the oxygen molecule (O_2) in its ground $^3\Sigma_g^-$, in the past target of several experimental studies, have been characterized under different theoretical points of view to clarify fundamental aspects of the intermolecular bond. For the most stable configuration of all Ng–O_2 systems, binding energy has been calculated at the theory's CCSD(T)/aug-cc-pVTZ level and compared with the experimental findings. Rovibrational energies, spectroscopic constants, and lifetime as a function of temperature were also evaluated by adopting properly formulated potential energy curves. The nature of the interaction involved was deeply investigated using charge displacement analysis, symmetry-adapted perturbation theory (SAPT), and natural bond orbital (NBO) methods. In all adducts, it was found that the charge transfer plays a minor role, although O_2 is an open shell species exhibiting a positive electron affinity. Obtained results also indicate that the dispersion attraction contribution is the main responsible for the complex stability.

Keywords: noble gas–O_2 adducts; spectroscopic constant; lifetime; charge transfer; energy decomposition

1. Introduction

Molecular interactions are essential in various areas of fundamental and applied research. The growing demand for new technologies has driven the study of weakly bound or long-range molecular complexes, controlled by non-covalent interactions, whose ubiquitous components are the van der Waals ones. Species with closed electronic shells, such as noble gas atoms, can form weakly bound stoichiometric aggregates (van der Waals) in the high-pressure regime. Several research groups have focused on understanding the stability and nature of the interatomic interactions involved in these complexes. Many phenomena have been observed in its dense metallic phases such as the appearance of electronic levels in the band gaps. This has been possible thanks to doping with atomic impurities that favor changes in electronic properties at low pressures [1]. In its ground electronic state $^3\Sigma_g^-$, O_2 is an open-shell paramagnetic molecule with a positive electron affinity and its interaction in different phases with other partners is of great relevance. In its singlet ground state, the gaseous dimer O_2–O_2 has been proposed by Lewis [2] as a prototype of the weak chemical bond (see also V. Aquilanti et al. [3]). Moreover, in the solid state, O_2 forms three phases with different ranges of stability and magnetic character (see V. Aquilanti et al. [3] and references therein). Experimental studies reveal that changes in crystallography and resistivity of platinum thin films (deposited by sputtering at increasing O_2 partial pressures) are enhanced by the use of Ne as a gas carrier. A slower deposition rate on Ne may allow more time for oxide formation in the substrate [4]. High-pressure experiments of the binary phase diagrams of O_2 with He, Ne, Ar, and Xe noble gas at 296 K

have been performed. The knowledge of these binary phase diagrams is very important as it provides a reference dataset to test theoretical calculations on mixtures, allows the growth of a single crystal of O_2 in a medium of the pressure of Ng, and also synthesizes oxides of Ng at high pressure. Furthermore, thermodynamic and structural properties of the mixtures of O_2 with Ng have been studied widely [5]. From a theoretical point of view, it is important and challenging to understand whether a van der Waals compound exists in any mixture of O_2 with Ng, as already experimentally observed for $Ar(H_2)_2$ [6], $Xe(H_2)_7$ [1], and $He(N_2)_{11}$ [7]. This knowledge can help in the synthesis of new molecular materials by pressure [5].

On the other hand, molecular interactions play a crucial role in different areas of knowledge. The growing demand for new technologies has driven the study of weakly bound (non-covalent) aggregates. In fact, the detailed characterization of the main component involved in a non-covalent interaction becomes fundamental in the identification and modeling of possible terms that compose the long-range or van der Waals-type forces [8,9]. This objective is very useful for evaluating the dynamic and static properties of these types of aggregates under a wide variety of possible applications. Gaseous $Ng–O_2$ systems have been the target of several investigations, exploiting essentially molecular beam scattering experiments which provided important details on range, strength, and anisotropy of the interaction (see F. Pirani et al. [10] and references therein). Moreover, in some particular cases, as $Ar–O_2$, some spectroscopic features of the IR spectrum (see, for instance, G. Henderson and G. Ewing [11]) have been also resolved. For $Ne–O_2$, the Zeeman spectrum has been measured [12]. In general, the characterization of important spectroscopic features and of the balance of the leading interaction components, determining the intermolecular bond strength and range in $Ng–O_2$, is still not completely available for the complete family of these weakly bound systems. In addition, several experimental findings suggest that $Ng–O_2$ represents a prototype of anisotropic van der Waals interaction, but a theoretical confirmation of this finding is still lacking, due to the difficulty to evaluate weak interactions in systems involving open-shell species.

Based on these reports, the present work presents a broad study involving the oxygen O_2 and the noble gases—Ng (Ng = He, Ne, Ar, Kr, Xe, and Rn). In more detail, exploring a series of different methodologies, the potential energy curves of the $Ng–O_2$ complexes, the charge displacement, the decomposition of electronic energy, the rovibrational energies, the spectroscopic constants, and the lifetime (as a function of temperature) were evaluated. With the determination of these important properties, it was possible to investigate the role and nature of the weak interaction in such compounds. The present investigation represents a continuation of a previous study on the structure and reactivity of noble gas compounds [13].

2. Methodologies and Computational Details

All the geometric variables used to describe the anisotropic interactions in $Ng–O_2$ systems are defined according to Figure 1. In this study, the interaction in the most stable configuration and the isotropic-spherical potential are both represented by the well-known Improved Lennard–Jones (ILJ) function [14] that provides in analytical form their radial dependence, that is, the dependence of involved interaction potential on the distance R between Ng atom and the center of mass of O_2.
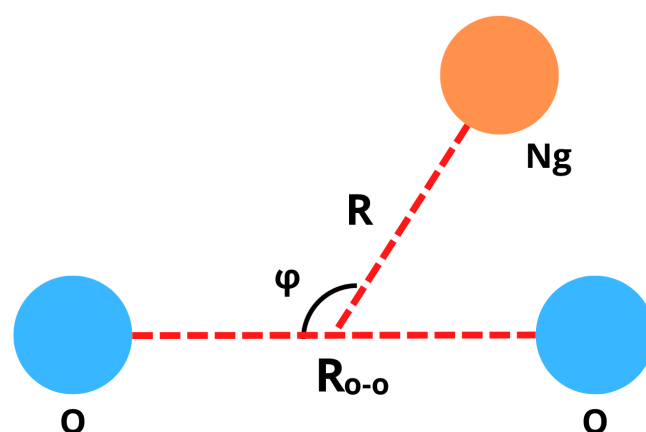
Figure 1. Geometric variables defining the structure of Ng–O$_2$ compounds.

For the case of a complex formed by two neutral species as Ng and O$_2$, the ILJ function is given by:

$$V(R) = D_e \left[\frac{6}{n(R) - 6} \left(\frac{R_e}{R} \right)^{n(R)} - \frac{n(R)}{n(R) - 6} \left(\frac{R_e}{R} \right)^6 \right]. \tag{1}$$

In the above equation, $n(R)$ is expressed by $\beta + 4 \left(\frac{R}{R_e} \right)^2$ and the β parameter reports the softness/hardness of the constituents that make up the adducts. Experimentally, this parameter assumes the value 9 for compounds involving noble gases [14]. Basically, to use Equation (1), the equilibrium distance (R_e) and the dissociation energy (D_e) must be known. R_e and D_e, associated with absolute minimum configurations of the complete family of Ng–O$_2$ compounds were determined by varying R distance and φ angle (between 0 and 180°) and keeping the intramolecular distance between oxygen atoms in O$_2$ fixed at the equilibrium position (R_{o-o} = 1.208 [15]), as represented in Figure 1. For each generated configuration, it was calculated the energy solving the electronic equation (within the Born–Oppenheimer approximation) at CCSD(T) [16,17] /aug-cc-pVTZ [18] level for He–O$_2$, Ne–O$_2$, Ar–O$_2$, and Kr–O$_2$ adducts. For the Xe–O$_2$ and Rn–O$_2$ compounds, the electronic energy was calculated at CCSD(T)/aug-cc-pVTZ-PP level. Furthermore, the basis set superposition error correction [19,20] was taken into account for all studied complexes. All calculations were performed via the Gaussian09 computational code [21]. Obtained D_e and R_e potential features are consistent with isotropic potential parameters predicted by empirical correlation formulas (ECF) [22] which provide the basic potential features for non-covalent interaction exploiting exclusively fundamental physical properties of interacting partners such as the electronic polarizability. In turn, predicted results agree with the experimental values extracted from the analysis of quantum interference effects resolved in scattering experiments and directly probing basic features of the interaction between projectile and target (see V. Aquilanti et al. [23] and reference therein). Therefore, present theoretical results have been used to perform an extensive and internally consistent analysis of the nature of the intermolecular interaction (see below). They have been exploited, together with results of ECF and Equation (1), to evaluate, in an internally consistent way, basic spectroscopic features for the complete family of systems.

The rovibrational spectroscopic constants (ω_e, $\omega_e x_e$, $\omega_e y_e$, α_e, and γ_e) were obtained using two different procedures. The first was the Dunham method [24], which is determined through the derivatives of potential energy curves in the equilibrium configuration. The second is given by the following equations [25]:

$$\omega_e = \frac{1}{24}[141(E_{1,0} - E_{0,0}) - 93(E_{2,0} - E_{0,0}) + 23(E_{3,0} - E_{1,0})]$$

$$\omega_e x_e = \frac{1}{4}[13(E_{1,0} - E_{0,0}) - 11(E_{2,0} - E_{0,0}) + 3(E_{3,0} - E_{1,0})]$$

$$\omega_e y_e = \frac{1}{6}[3(E_{1,0} - E_{0,0}) - 3(E_{2,0} - E_{0,0}) + (E_{3,0} - E_{1,0})] \tag{2}$$

$$\alpha_e = \frac{1}{8}[-12(E_{1,1} - E_{0,1}) + 4(E_{2,1} - E_{0,1}) + 4\omega_e - 23\omega_e y_e]$$

$$\gamma_e = \frac{1}{4}[-2(E_{1,1} - E_{0,1}) + (E_{2,1} - E_{0,1}) + 2\omega_e x_e - 9\omega_e y_e].$$

In Equation (2), $E_{v,j}$ expresses the rovibrational energy where v and j represent the vibrational and rotational quantum numbers, respectively. In this work, $E_{v,j}$ were calculated by solving the nuclear Schrödinger equation using the Discrete Variable Representation method [26].

The description of the nature of the intermolecular bond of O_2–Ng adducts was based on the definition of charge displacement along a direction (z-axis, for example) and is defined by the following equation [27–30]:

$$\Delta q(z) = \int_{-\infty}^{\infty} dx \int_{-\infty}^{\infty} dy \int_{-\infty}^{z} \Delta \rho(x, y, z')dz', \tag{3}$$

where Δq is the density difference between the compound and the two separated parts (O_2 and noble gas) arranged in the same positions they occupy in the compound. We emphasize that canonical charge decomposition methods cannot be used since they provide inaccurate results for Δq when the charge displacement is small [31]. The z-axis that appears in Equation (3) joins the bonding center of the O_2 molecule (located at the origin of the z-axis) with the noble gas (located in the negative part of the z-axis). Accordingly, Δq determines at each z-position the electron charge that is moved from the right to the left side along the negative z-axis. In this way, the displacement of charge takes place from the Ng to the oxygen dimer when $\Delta q(z)$ is negative. If $\Delta q(z)$ is positive, then the electron charge occurs from O_2 to Ng. Equation (3) was solved using the Multiwfn computational package [32].

With the aim of individualizing the contribution of the terms (Electrostatic E_{elect}, induction E_{ind}, dispersion E_{disp}, and exchange E_{exch}) that compose the interaction involved in the Ng–O_2 complexes, the symmetry-adapted perturbation theory (SAPT) [33] method was used at sapt2+3(CCD)/aug-cc pVTZ [18] level as implemented in the PSI4 [34,35] computational code. In order to describe the origin of the electronic rearrangements of the Ng–O_2 complexes in detail, the analysis of the natural bond orbital (NBO) was also used [36]. All NBO calculations were performed at CCSD(T) [16,17]/aug-cc-pVTZ [18] level by using the Gaussian09 package [21]. For Xe–O_2 and Rn–O_2 complexes, aug-cc-pVTZ-PP were employed.

Finally, the lifetimes as a function of the temperature of all Ng–O_2 complexes were determined using Slater's theory and it is given by expression [37,38]:

$$\tau(T) = \frac{1}{\omega_e} e^{\frac{D_e - E_{0,0}}{R_g T}}, \tag{4}$$

where $E_{0,0}$ stands for zero point energy (the rovibrational energy calculated for $v = 0$ and $j = 0$), T is the temperature, and R_g is the universal gas constant. This description assumes that the unimolecular decomposition of the aggregate occurs when the interaction coordinate arrives at the dissociation threshold (D_e).

3. Results and Discussion

Table 1 shows the CCSD/aug-cc-pVDZ optimized geometric parameters (R_e and φ) and the CCSD(t)/aug-cc-pVTZ corresponding energy (D_e) that describe the most stable

configuration of all atom–molecule complexes formed by Ng and O_2. The single reference coupled cluster calculation for the closed shell system is considered reliable if the T1 diagnostic value is below 0.020 [39,40]. The T1 values for all systems investigated show that there is no multireference character, and it decreases from He to Rn as follows: He–O_2 (0.0141), Ne–O_2 (0.0128), Ar–O_2 (0.0119), Kr–O_2 (0.0099), Xe–O_2 (0.0099), and Rn–O_2 (0.0091). These results were compared with those obtained via the ECF procedure [9,22]. ECF makes use of a generalized connection between the potential parameters involved in a van der Waals interaction, with polarizabilities and the number of valence electrons (from the fragments of the complexes) that are effectively perturbed by the interaction. Comparing the two results, it is noted that the greatest (smallest) difference found for R_e and D_e was 0.28 Å (0.08 Å) for He–O_2 (Xe–O_2), and 1.62 meV $\approx$ 0.037 kcal/mol (0.00 meV) for Rn–O_2 (Xe–O_2), respectively. This comparison indicates that there is a good agreement between the R_e e D_e results obtained by the two methodologies. This fact indicates that the potential energy curves (PEC), for each complex, constructed from the substitution of the values of $\beta = 9.0$, R_e and D_e (Table 1) in Equation (1) are suitable for describing the electronic and dynamic properties of Ng–O_2 compounds. The corresponding PECs are shown in Figures 2 and 3. Another essential fact that deserves to be highlighted is the excellent agreement between the experimental ($\varphi = 90°$) and theoretical angles of the most stable approach of He ($\varphi = 89.9°$) and Ar ($\varphi = 88.8°$) to the binding center of the O_2 molecule ([10] and references therein and [41]).

Table 1. Geometric parameters (R_e and φ) of the most stable configurations and corresponding energies (D_e) of the Ng–O_2 complexes. The values in parentheses refer to the results available in the literature which were determined via the ECF approach [9,22] (see text for more details). The μ reduced masses of each complex are also shown.

Complexes	R_e (Å)	D_e (meV)	φ (°)	μ (a.u)
He–O_2	3.17 (3.45)	3.75 (2.91)	89.9	6309.80486
Ne–O_2	3.36 (3.52)	5.11 (5.88)	80.0	22,558.61103
Ar–O_2	3.67 (3.79)	10.84 (11.78)	88.8	32,374.47312
Kr–O_2	3.78 (3.91)	14.56 (14.26)	81.0	42,210.71200
Xe–O_2	4.01 (4.09)	16.04 (16.04)	81.0	46,896.81884
Rn–O_2	4.06 (4.19)	16.84 (18.46)	81.0	52,658.65576

Using the PECs from Figures 2 and 3, the reduced masses from Table 1, and the procedure described in Section 2, it was possible to determine the rovibrational energies of the Ng–O_2 complexes as presented in Tables 2 and 3. From these tables, it is important to note that both He–O_2 PECs admit only one confined vibrational level within its potential well. This happens probably due to the small values of the dissociation energy (D_e) and reduced mass of the He–O_2 compound. The number of levels obtained with the different types of potential energy curves is the same, except for Ne–O_2, Ar–O_2, and Rn–O_2, where the potential well of PEC ECF contains one more level than CSDD(T) PEC. Tables 4 and 5 show the rovibrational spectroscopic constants obtained by both the Dunham method and Equation (2). From these tables, one can see a good agreement between the two methodologies. This agreement is important because it brings more confidence in the obtained results since, as far as we know, there are no literature data for comparison. Note that for the compounds He–O_2 (which has only one vibrational level inside its potential well) and Ne–O_2 (which has only three vibrational levels inside its potential well), there was no possibility to calculate the spectroscopic constants via Equation (2), because to use it, at least four vibrational levels are needed.
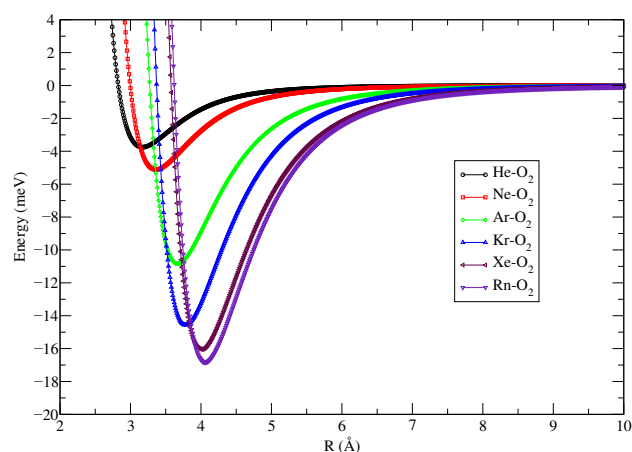
Figure 2. Improved Lennard Jones potential energy curves for the Ng–O$_2$ compounds obtained at CCSD(t)/aug-cc-pVTZ level with the BSSE correction.
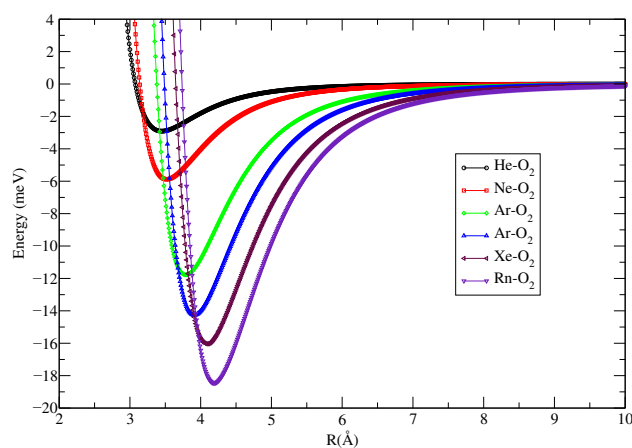

Figure 3. Improved Lennard Jones potential energy curves for the Ng–O$_2$ compounds obtained through the ECF approach.

Table 2. Vibrational ($j = 0$) and rovibrationl ($j = 1$) energies in cm^{-1} for the Ng–O$_2$ complexes obtained through CCSD(T)/aug-cc-pVTZ potential energy curve.

v	j	He–O$_2$	Ne–O$_2$	Ar–O$_2$	Kr–O$_2$	Xe–O$_2$	Rn–O$_2$
0	0	21.3536	13.2550	14.7518	14.7332	13.9043	13.3169
1	0	-	30.9952	39.6642	40.8599	39.0358	37.6220
2	0	-	39.2232	58.7146	62.6703	60.6929	58.8989
3	0	-	-	72.2600	80.3115	78.9669	77.2163
4	0	-	-	80.8756	93.9888	93.9772	92.6617
5	0	-	-	85.4532	103.9947	105.8846	105.3487
6	0	-	-	-	110.7416	114.9070	115.4270
7	0	-	-	-	114.7757	121.3358	123.0943
8	0	-	-	-	116.8906	125.5402	128.6035
9	0	-	-	-	-	128.0208	132.2635
10	0	-	-	-	-	-	134.5124
0	1	22.0513	13.4736	14.8871	14.8320	13.9837	13.3861
1	1	-	31.1662	39.7873	40.9526	39.1111	37.6879
2	1	-	39.3342	58.8238	62.7560	60.7636	58.9612
3	1	-	-	72.3532	80.3898	79.0326	77.2748
4	1	-	-	80.9502	94.0586	94.0376	92.7161
5	1	-	-	85.5065	104.0551	105.9391	105.3986
6	1	-	-	-	110.7916	114.9551	115.4721
7	1	-	-	-	114.8142	121.3767	123.1341
8	1	-	-	-	116.9200	125.5735	128.6377
9	1	-	-	-	-	128.0470	132.2914
10	1	-	-	-	-	-	134.5351

Table 3. Vibrational ($j = 0$) and rovibrational ($j = 1$) energies in cm^{-1} for the Ng–O$_2$ complexes obtained through the ECF potential energy curve.

v	j	He–O$_2$	Ne–O$_2$	Ar–O$_2$	Kr–O$_2$	Xe–O$_2$	Rn–O$_2$
0	0	15.3999	13.1298	14.9448	14.1078	13.6404	13.5385
1	0	-	32.3170	40.5221	39.2010	38.3479	38.4275
2	0	-	42.9573	60.5738	60.2558	59.7129	60.4665
3	0	-	46.9871	75.3899	77.4049	77.8210	79.7135
4	0	-	-	85.4212	90.8305	92.7828	96.2402
5	0	-	-	91.3598	100.7913	104.7460	110.1375
6	0	-	-	94.2410	107.6498	113.9102	121.5227
7	0	-	-	-	111.8883	120.5411	130.5474
8	0	-	-	-	114.2040	124.9771	137.4060
9	0	-	-	-	-	127.6664	142.3384
10	0	-	-	-	-	-	145.6317
11	0	-	-	-	-	-	147.8315
0	1	16.0302	13.3341	15.0720	14.2003	13.7171	13.6037
1	1	-	32.4855	40.6387	39.2878	38.4204	38.4897
2	1	-	43.0807	60.6786	60.3364	59.7811	60.5256
3	1	-	47.0579	75.4811	77.4785	77.8846	79.7694
4	1	-	-	85.4970	90.8966	92.8413	96.2926
5	1	-	-	91.4178	100.8489	104.7990	110.1862
6	1	-	-	94.2820	107.6981	113.9572	121.5672
7	1	-	-	-	111.9263	120.5815	130.5876
8	1	-	-	-	114.2332	125.0104	137.4415
9	1	-	-	-	-	127.6928	142.3687
10	1	-	-	-	-	-	145.6567
11	1	-	-	-	-	-	147.8534

Table 4. Ng–O$_2$ spectroscopic constants (cm^{-1}) obtained through the CCSD(T)/aug-cc-pVTZ potential energy curve.

Constants	He–O$_2$	Ne–O$_2$	Ar–O$_2$	Kr–O$_2$	Xe–O$_2$	Rn–O$_2$
ω_e (Equation (2))	-	-	31.11	30.58	28.69	27.40
ω_e (Dunham)	47.81	29.69	31.00	30.56	28.67	27.38
$\omega_e x_e$ (Equation (2))	-	-	3.19	2.27	1.80	1.56
$\omega_e x_e$ (Dunham)	21.90	5.32	3.10	2.23	1.79	1.55
$\omega_e y_e$ (Equation (2))	-	-	5.95×10^{-2}	2.46×10^{-2}	1.50×10^{-3}	1.15×10^{-2}
$\omega_e y_e$ (Dunham)	0.84	8.46×10^{-2}	2.76×10^{-2}	1.46×10^{-2}	1.00×10^{-2}	7.90×10^{-3}
α_e (Equation (2))	-	-	5.31×10^{-3}	2.87×10^{-3}	1.96×10^{-3}	1.56×10^{-3}
α_e (Dunham)	0.16	1.68×10^{-2}	5.49×10^{-3}	2.91×10^{-3}	1.98×10^{-3}	1.56×10^{-3}
γ_e (Equation (2))	-	-	4.08×10^{-4}	1.42×10^{-4}	8.13×10^{-5}	5.55×10^{-5}
γ_e (Dunham)	3.72×10^{-2}	1.48×10^{-3}	2.72×10^{-4}	1.05×10^{-4}	6.15×10^{-5}	4.42×10^{-5}

Table 5. Ng–O$_2$ spectroscopic constants (cm^{-1}) obtained through the ECF potential energy curve.

Constants	He–O$_2$	Ne-O$_2$	Ar–O$_2$	Kr–O$_2$	Xe–O$_2$	Rn–O$_2$
ω_e (Equation (2))	-	29.59	31.38	29.26	28.13	27.79
ω_e (Dunham)	38.70	28.52	31.29	29.23	28.11	27.78
$\omega_e x_e$ (Equation (2))	-	5.72	2.98	2.12	1.73	1.47
$\omega_e x_e$ (Dunham)	18.54	4.84	2.90	2.09	1.72	1.46
$\omega_e y_e$ (Equation (2))	-	0.32	4.83×10^{-2}	2.21×10^{-2}	1.42×10^{-2}	9.67×10^{-3}
$\omega_e y_e$ (Dunham)	0.74	7.31	2.40×10^{-3}	1.33×10^{-2}	9.42×10^{-3}	6.86×10^{-3}
α_e (Equation (2))	-	1.32×10^{-2}	4.65×10^{-3}	2.62×10^{-3}	1.85×10^{-3}	1.35×10^{-3}
α_e (Dunham)	0.14	1.45×10^{-2}	4.78×10^{-3}	2.66×10^{-3}	1.87×10^{-3}	1.36×10^{-3}
γ_e (Equation (2))	-	2.36×10^{-3}	3.21×10^{-4}	1.26×10^{-4}	7.26×10^{-5}	4.38×10^{-5}
γ_e (Dunham)	3.41×10^{-2}	1.22×10^{-3}	2.20×10^{-3}	1.49×10^{-5}	5.68×10^{-5}	3.55×10^{-5}

Figure 4 shows the calculated charge displacement (Δq) for all Ng–O_2 adducts in their most stable configuration. From this Figure, one can see that Δq becomes appreciably different from zero only when Ng is very close to O_2. However, in all cases, Δq changes sign within the intermolecular distance, and only for Ar–O_2, it maintains a very small negative value in an appreciable z range. All these features represent a clear indication that the charge transfer plays a practically null role in determining the weak intermolecular bond [27–30].
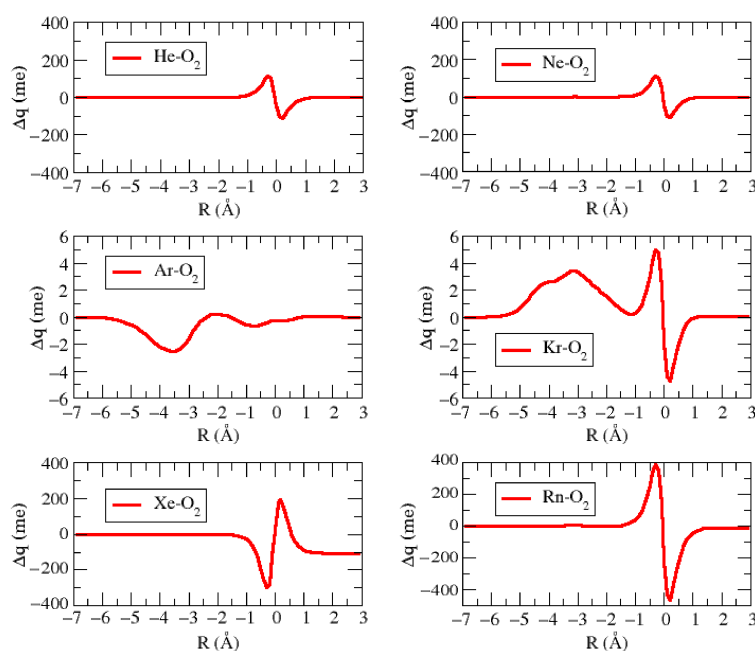
Figure 4. Charge Displacement (Δq) pictures for the most stable configuration for the Ng–O_2 complexes.

Table 6 shows the interaction energy decomposition of the Ng–O_2 complexes calculated at sapt2+3(CCD)/aug-cc-pVTZ level. From this table, it is possible to observe that the dispersion term (E_{disp}) overcomes in all Ng–O_2 adducts, with a higher/lower contribution of 82.2%/75.6% for the Ar–O_2/Ar–O_2 complexes. This fact suggests that all Ng–O_2 complexes are basically governed by a non-covalent or van der Waals-type interaction, where exchange repulsion and dispersion attraction represent the leading components. Table 7 reports the second-order perturbation energies (E^2) obtained through the NBO analysis for the Ng–O_2 complexes. First, the results presented in this table reveal that the electronic donation between the Ne atom and the O_2 oxygen dimer is practically negligible with E^2 less than 0.05 kcal/mol. In addition, a very small electronic donation takes place from the oxygen 1-center valence lone pair orbital (LP) to the 1-center antibond orbital of Rydberg (RY*) of the He, Kr, Xe, and Rn noble gases. For the Ar–O_2, an small electronic donation also happens from the O–O bond orbital (BD), located on O_2 dimer, to the 1-center antibond orbital of Rydberg (RY*) of the Ar atom. In any case, these values are very small and consistent with the charge displacement results of Figure 3. This combined analysis confirms the nature of van der Waals for all these systems.

Figures 5 and 6 present the lifetime as a function of temperature for all complexes obtained through CCSD(T) and ECF PECs, respectively. The first indication of these figures is that the He–O_2 complex has a lifetime of less than one second for the entire temperature range from 200 to 500 K. In this case, according to Wolfgang [42], the potential energy well is not deep enough to exclude the intermediate complex and so the adduct is considered unstable. For the other complexes, the lifetime was slightly above 1 picosecond for the entire considered temperature range, indicating that these systems are weakly bound. These facts are in line with the results obtained with the charge displacement, NBO analysis, and SAPT calculations.

Table 6. Interaction energy decomposition (given in Kcal/mol) of the Ng–O$_2$ complexes calculated at the sapt2+3(CCD)/aug-cc-pVTZ level.

Terms	He–O$_2$	Ne–O$_2$	Ar–O$_2$	Kr–O$_2$	Xe–O$_2$	Rn–O$_2$
E$_{elect}$	−0.0062	−0.035	−0.1141	−0.1571	−0.0776	−0.1022
E$_{exch}$	0.0342	0.1449	0.3539	0.4578	0.2543	0.3224
E$_{ind}$	−0.0014	−0.0024	−0.015	−0.0229	−0.0176	−0.0231
E$_{disp}$	−0.0900	−0.2457	−0.5407	−0.6381	−0.4416	−0.4977
%E$_{elect}$	13.8%	13.7%	17.0%	19.2%	13.6%	16.4%
%E$_{ind}$	10.6%	9.5%	2.3%	2.8%	3.2%	3.7%
%E$_{disp}$	75.6%	76.8%	80.7%	78.0%	82.2%	79.9%

Table 7. Natural bond orbital population analysis obtained through second-order perturbation energies (E^2) at the CCSD(T)/aug-cc-pVTZ level for the Ng–O$_2$ complexes.

Complexes	Donor	Receptor	E^2(kcal/mol)
He–O$_2$	LP(2) O2	RY*(1) He	0.06
Ne–O$_2$	-	-	-
Ar–O$_2$	BD(2) O1-O2	RY*(1) Ar	0.12
Kr-O$_2$	LP(2) O1 LP(2) O2	RY*(1) Kr RY*(1) Kr	0.05 0.06
Xe–O$_2$	LP(2) O1 LP(2) O2	RY*(1) Xe RY*(1) Xe	0.06 0.06
Rn–O$_2$	LP(2) O1 LP(2) O2	RY*(2) Rn RY*(1) Rn	0.06 0.06
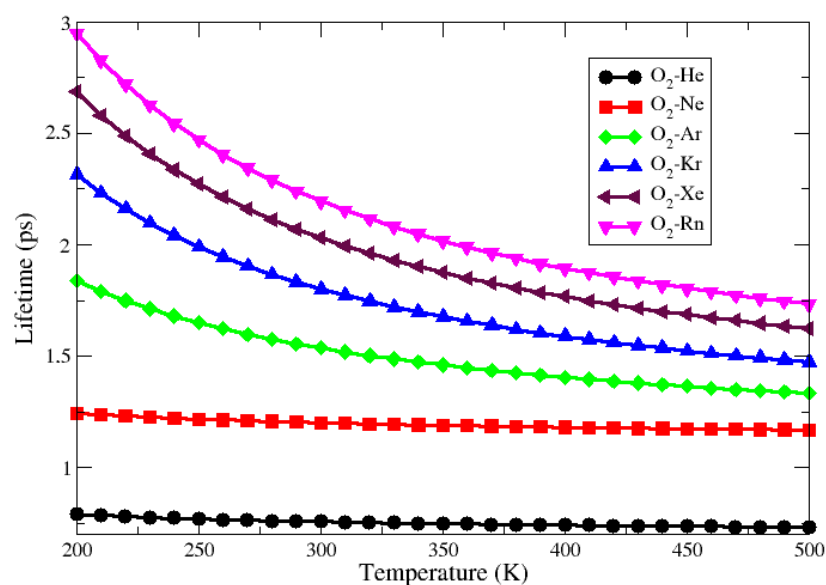
Figure 5. Lifetime behavior as a function of temperature for a Ng–O$_2$ compounds obtained at CCSD(t)/aug-cc-pVTZ level.
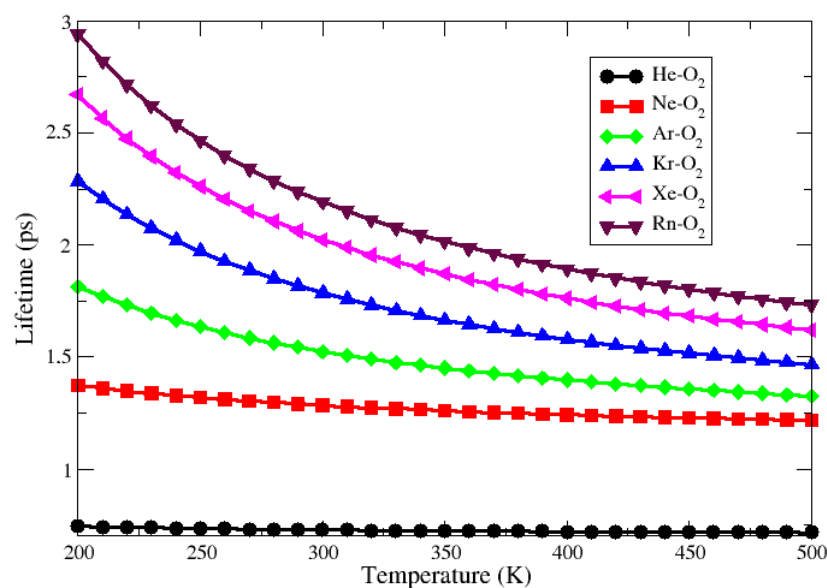
Figure 6. Lifetime behavior as a function of temperature for the Ng–O$_2$ compounds obtained through ECF approach.

4. Conclusions

The present theoretical investigation proves that Ng–O$_2$ aggregates are effectively bound by van der Waals interactions. Although O$_2$ in its ground electronic state ($^3\Sigma_g^-$) is an open-shell species with positive electron affinity, the present analysis confirms the experimental finding that its interaction with Ng atoms is not affected by charge transfer component, even in adducts formed by O$_2$ with heavier Ng. It is also confirmed that in all systems the T (perpendicular) is the most stable configuration. The phenomenological potentials, which correctly reproduce interference effects in scattering experiments that are depending on specific features of the potential well, are here used, together with ab initio calculations of the intermolecular interaction, to evaluate roto-vibration spectroscopic features of Ng–O$_2$ complexes in the range of temperatures 200–500 K. It is found that only He–O$_2$ is unstable under the selected conditions of the bulk. The knowledge acquired in the present study about the non-covalent character (van der Waals) of the mixture of O$_2$ and Noble gas can be useful in the synthesis of new molecular materials by pressure.

References

1. Somayazulu, M.; Dera, P.; Goncharov, A.F.; Gramsch, S.A.; Liermann, P.; Yang, W.; Liu, Z.; Mao, H.-k.; Hemley, J.R. Pressure-induced bonding and compound formation in xenon-hydrogen solids. *Nat. Chem.* **2010**, *2*, 50–53. [CrossRef] [PubMed]
2. Lewis, G.N. The magnetism of oxygen and the molecule O$_4$. *J. Am. Chem. Soc.* **1924**, *46*, 2027–2032. [CrossRef]

3. Aquilanti, V.; Ascenzi, D.; Bartolomei, M.; Cappelletti, D.; Cavalli, S.; Vitores, M.C.; Pirani, F. Molecular Beam Scattering of Aligned Oxygen Molecules. The Nature of the Bond in the O_2-O_2 Dimer. *J. Am. Chem. Soc.* **1999**, *121*, 10794–10802. [CrossRef]
4. Aita, C.R.; Tran, N.C. Rare gas-oxygen effects on the rf sputter deposition of platinum. *J. Appl. Phys.* **1983**, *54*, 6051–6052. [CrossRef]
5. Weck, G.; Dewaele, A.; Loubeyre, P. Oxygen/noble gas binary phase diagrams at 296 K and high pressures. *Phys. Rev. B* **2010**, *82*, 014112. [CrossRef]
6. Loubeyre, P.; Letoullec, R.; Pinceaux, J.P. Compression of $Ar(H_2)_2$ up to 175 GPa: A New Path for the dissociation of Molecular Hydrogen? *Phys. Rev. Lett.* **1994**, *72*, 1360–1365. [CrossRef]
7. Vos, W.L.; Finger, L.W.; Hemley, R.J.; Hu, J.Z.; Mao, H.K.; Schouten, J.A. A high-pressure van der Waals compound in solid nitrogen-helium mixtures. *Nature* **1992**, *358*, 46–48. [CrossRef]
8. Cappelletti, D.; Vilela, A.F.; Barreto, P.R.; Gargano, R.; Pirani, F.; Aquilanti, V. Intermolecular interactions of H_2S with rare gases from molecular beam scattering in the glory regime and from ab initio calculations. *J. Chem. Phys.* **2006**, *125*, 133111. [CrossRef]
9. Pirani, F.; Maciel, G.S.; Cappelletti, D.; Aquilanti, V. Experimental benchmarks and phenomenology of interatomic forces: open-shell and electronic anisotropy effects. *Int. Rev. Phys. Chem.* **2006**, *25*, 165–199. [CrossRef]
10. Pirani, F.; Cappelletti, D.; Falcinelli, S.; Cesario, D.; Nunzi, F.; Belpassi, L.; Tarantelli, F. Selective Emergence of the Halogen Bond in Ground and Excited States of Noble-Gas–Chlorine Systems. *Angew. Chem. Int. Ed.* **2019**, *58*, 4195–4199. [CrossRef]
11. Henderson, G.; Ewing, G.E. Infrared spectrum, structure, and properties of the O_2–Ar van der Waals molecule. *J. Chem. Phys.* **1973**, *59*, 2280–2293. [CrossRef]
12. Beneventi, L.; Casavecchia, P.; Pirani, F.; Vecchiocattivi, F.; Volpi, G.G. The Ne–O_2 potential energy surface from high-resolution diffraction and glory scattering experiments and from the Zeeman spectrum. *J. Chem. Phys.* **1991**, *95*, 195–204. [CrossRef]
13. Nunzi, F.; Pannacci, G.; Tarantelli, F.; Belpassi, L.; Cappelletti, D.; Falcinelli, S.; Pirani, F. Leading interaction components in the structure and reactivity of noble gases compounds. *Molecules* **2020**, *25*, 2367. [CrossRef] [PubMed]
14. Pirani, F.; Brizi, S.; Roncaratti, L.; Casavecchia, P.; Cappelletti, D.; Vecchiocattivi, F. Beyond the Lennard-Jones model: A simple and accurate potential function probed by high resolution scattering data useful for molecular dynamics simulations. *Phys. Chem. Chem. Phys.* **2008**, *10*, 5489–503. [CrossRef] [PubMed]
15. Radzig, A.A.; Smirnov, B.M. *Reference Data on Atoms, Molecules, and Ions*; Springer: Berlin/Heidelberg, Germany, 1985.
16. Rittby, M.; Bartlett, R.J. An open-shell spin-restricted coupled cluster method: application to ionization potentials in nitrogen. *J. Phys. Chem.* **1988**, *92*, 3033–3036. [CrossRef]
17. Watts, J.D.; Gauss, J.; Bartlett, R.J. Open-shell analytical energy gradients for triple excitation many-body, coupled-cluster methods: MBPT (4), CCSD+ T (CCSD), CCSD (T), and QCISD (T). *Chem. Phys. Lett.* **1992**, *200*, 1–7. [CrossRef]
18. Peterson, K.A.; Woon, D.E.; Dunning, T.H., Jr. Benchmark calculations with correlated molecular wave functions. IV. The classical barrier height of the $H + H_2 \rightarrow H_2 + H$ reaction. *J. Chem. Phys.* **1994**, *100*, 7410–7415. [CrossRef]
19. Kállay, M.; Surján, P.R. Higher excitations in coupled-cluster theory. *J. Chem. Phys.* **2001**, *115*, 2945–2954. [CrossRef]
20. Simon, S.; Duran, M.; Dannenberg, J. How does basis set superposition error change the potential surfaces for hydrogen-bonded dimers? *J. Chem. Phys.* **1996**, *105*, 11024–11031. [CrossRef]
21. Frisch, M.J.; Trucks, G.W.; Schlegel, H.B.; Scuseria, G.E.; Robb, M.A.; Cheeseman, J.R.; Scalmani, G.; Barone, V.; Petersson, G.A.; Nakatsuji, H.; et al. *Gaussian09 Revision A.02*; Gaussian Inc.: Wallingford, CT, USA, 2016.
22. Cambi, R.; Cappelletti, D.; Liuti, G.; Pirani, F. Generalized correlations in terms of polarizability for van der Waals interaction potential parameter calculations. *J. Chem. Phys.* **1991**, *95*, 1852–1861. [CrossRef]
23. Aquilanti, V.; Cornicchi, E.; Teixidor, M.M.; Saendig, N.; Pirani, F.; Cappellett, D. Glory-Scattering Measurement of Water-Noble-Gas Interactions: The Birth of the Hydrogen Bond. *Angew. Chem. Int. Ed.* **2005**, *44*, 4239–4243. [CrossRef] [PubMed]
24. Dunham, J.L. The Energy Levels of a Rotating Vibrator. *Phys. Rev.* **1932**, *41*, 721–731. [CrossRef]
25. da Cunha, W.F.; de Oliveira, R.M.; Roncaratti, L.F.; Martins, J.B.; e Silva, G.M.; Gargano, R. Rovibrational energies and spectroscopic constants for H$_2$O-Ng complexes. *J. Mol. Model.* **2014**, *20*, 2498. [CrossRef] [PubMed]
26. Prudente, F.; Costa, L.; Neto, J.S. Discrete variable representation and negative imaginary potential to study metastable states and photodissociation processes. Application to diatomic and triatomic molecules. *J. Mol. Struct. THEOCHEM* **1997**, *394*, 169–180. [CrossRef]
27. Cappelletti, D.; Ronca, E.; Belpassi, L.; Tarantelli, F.; Pirani, F. Revealing Charge-Transfer Effects in Gas-Phase Water Chemistry. *Acc. Chem. Res.* **2012**, *45*, 1571–1580. [CrossRef]
28. Belpassi, L.; Infante, I.; Tarantelli, F.; Visscher, L. The chemical bond between *Au* (*I*) and the noble gases. Comparative study of *NgAuF* and $NgAu^+$ ($Ng = Ar, Kr, Xe$) by density functional and coupled cluster methods. *J. Am. Chem. Soc.* **2008**, *130*, 1048–1060. [CrossRef]
29. Belpassi, L.; Tarantelli, F.; Pirani, F.; Candori, P.; Cappelletti, D. Experimental and theoretical evidence of charge transfer in weakly bound complexes of water. *Phys. Chem. Chem. Phys.* **2009**, *11*, 9970–9975. [CrossRef]
30. Pirani, F.; Candori, P.; Mundim, M.P.; Belpassi, L.; Tarantelli, F.; Cappelletti, D. On the role of charge transfer in the stabilization of weakly bound complexes involving water and hydrogen sulphide molecules. *Chem. Phys.* **2012**, *398*, 176–185. [CrossRef]
31. Belpassi, L.; Reca, M.L.; Tarantelli, F.; Roncaratti, L.F.; Pirani, F.; Cappelletti, D.; Faure, A.; Scribano, Y. Charge-Transfer Energy in the Water- Hydrogen Molecular Aggregate Revealed by Molecular-Beam Scattering Experiments, Charge Displacement Analysis, and ab Initio Calculations. *J. Am. Chem. Soc.* **2010**, *132*, 13046–13058. [CrossRef]

32.   Lu, T.; Chen, F. Multiwfn: A multifunctional wavefunction analyzer. *J. Comput. Chem.* **2012**, *33*, 580–592. [CrossRef]
33.   Jeziorski, B.; Moszynski, R.; Szalewicz, K. Perturbation theory approach to intermolecular potential energy surfaces of van der Waals complexes. *Chem. Rev.* **1994**, *94*, 1887–1930. [CrossRef]
34.   Turney, J.M.; Simmonett, A.C.; Parrish, R.M.; Hohenstein, E.G.; Evangelista, F.A.; Fermann, J.T.; Mintz, B.J.; Burns, L.A.; Wilke, J.J.; Abrams, M.L.; et al. Psi4: An open-source ab initio electronic structure program. *Wiley Interdiscip. Rev. Comput. Mol. Sci.* **2012**, *2*, 556–565. [CrossRef]
35.   Smith, D.G.; Burns, L.A.; Simmonett, A.C.; Parrish, R.M.; Schieber, M.C.; Galvelis, R.; Kraus, P.; Kruse, H.; Di Remigio, R.; Alenaizan, A.; et al. PSI4 1.4: Open-source software for high-throughput quantum chemistry. *J. Chem. Phys.* **2020**, *152*, 184108. [CrossRef] [PubMed]
36.   Weinhold, F. Natural bond orbital analysis: A critical overview of relationships to alternative bonding perspectives. *J. Comput. Chem.* **2012**, *33*, 2363–2379. [CrossRef] [PubMed]
37.   Slater, J.C. *The Rates of Unimolecular Reactions in Gases*; Cambridge University Press: Cambridge, UK, 1939; Volume 35, p. 56.
38.   Laidler, K.L. *Theories of Chemical Reaction Rates*; McGraw-Hill: New York, NY, USA, 1969.
39.   Lee, T.J.; Taylor, P.R. A diagnostic for determining the quality of single-reference electron correlation methods. *Int. J. Quantum Chem.* **1989**, *36*, 199–207. [CrossRef]
40.   Lee, T.J. Comparison of the T1 and D1 diagnostics for electronic structure theory: A new definition for the open-shell D1 diagnostic. *Chem. Phys. Lett.* **2003**, *372*, 362–367. [CrossRef]
41.   Pirani, F.; Vecchiocattivi, F. The interaction potential energy surface of O2-Ar. *Chem. Phys.* **1981**, *59*, 387–396. [CrossRef]
42.   Wolfgang, R. Energy and chemical reaction. II. Intermediate complexes vs. direct mechanisms. *Acc. Chem. Res.* **1970**, *3*, 48–54. [CrossRef]